ACS Sustainable Chemistry & Engineering

Research Article

Cite This: ACS Sustainable Chem. Eng. 2018, 6, 12953−12960

pubs.acs.org/journal/ascecg

Enhanced Charge Separation of TiO_2 Nanotubes Photoelectrode for Efficient Conversion of CO_2

Jing Wu,[†] Da Li,[†] Jia Liu,*[,†] Chao Li,[†] Zeng Li,[†] Bruce E. Logan,[‡] and Yujie Feng*[,†]

[†]State Key Laboratory of Urban Water Resource and Environment, Harbin Institute of Technology, No 73 Huanghe Road, Nangang District, Harbin 150090, China

[‡]Department of Civil and Environmental Engineering, Penn State University, 212 Sackett Building, University Park, Pennsylvania 16802, United States

Supporting Information

ABSTRACT: For the production of TiO_2 nanotubes (TNTs) efficient photoelectrodes they must have efficient charge separation by trapping holes and transfer of electrons. In this study, MnO_x and Pd codecorated TNTs photoelectrodes were successfully constructed using a simple impregnation method, followed by an electrochemical deposition process. The photocatalytic activities for CO_2 conversion by the optimized TNTs photoelectrode (10Pd/0.8Mn/TNTs) were increased by 2.8 times to produce 40.3 ± 2.5 mg L^{-1} acetic acid, and by 2.5 times to generate 24.6 ± 1.9 mg L^{-1} formic acid compared to a bare TNTs photoelectrode. The optimized photoelectrode also showed the highest transient photocurrent of 1.15 mA cm^{-2}. The improved performance was due to the elevated charge separation through bidirectional modulation of photogenerated holes and electrons, on the basis of the steady-state surface photovoltage and analysis with the formed •OH concentrations, electrochemical reduction tests with N_2 or CO_2 atmospheres, and electrochemical impedance spectra. The decorated MnO_x effectively trapped the photogenerated holes, and the decorated Pd facilitated photogenerated electron transfer and promoted visible light absorption. The decorated MnO_x and Pd also played catalytic roles in the redox reactions involved with the photogenerated charge carriers.

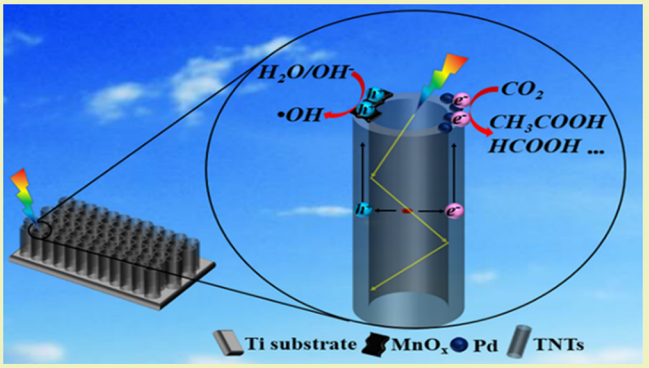

KEYWORDS: *TiO_2 nanotubes, Trapping holes, Transferring electrons, MnO_x, Pd*

INTRODUCTION

The conversion of CO_2 to green and valuable chemicals has aroused extensive interest from the viewpoint of both capturing CO_2 as well as producing useful chemicals.[1−4] Among the different techniques being used to convert CO_2 into useful products, semiconductor photocatalysis is of particular interest due to multiple advantages of using inexpensive materials, showing good stability, and using sunlight.[5−7] Among the many photocatalysts being investigated, TiO_2 is of particular interest due to a lack of chemical toxicity, strong oxidation ability, low cost, and effectiveness.[8−10] TiO_2 nanotubes TNTs) with a one-dimensional highly ordered nanostructure have further advantages due to their larger specific surface area, more active sites, and improved light-harvesting properties compared to TiO_2 nanoparticles and nanofilms.[11−13] However, applications of TNTs are still limited because of their wide band gap and a low separation of photogenerated electrons and holes.[14] Therefore, research has focused on overcoming these limitations and elevating the performance of TNTs materials.

The main research methods being pursued to improve the performance of TNTs are decoration with metal oxides, noble metal cocatalyst deposition, and constructing heterostructures with another semiconductor.[15−17] By decorating TNTs with certain ratios of metal oxides (MO_x) for the function of trapping holes, photogenerated charge separation can be elevated.[18,19] MnO_x has been shown to greatly benefit water oxidation because of its multiple valence states, capacity for capturing photogenerated holes, abundance in nature, and low toxicity.[20−22] Therefore, MnO_x should be a good candidate to control holes on TNTs and improve its photocatalytic performance.[23−25] With the deposition of a noble metal, photogenerated electron transfer can be elevated, and the adsorption of visible light could also be enhanced, resulting in an enhanced charge separation.[17,26] For example, palladium can not only elevate light adsorption ability, but also accept photogenerated electrons from the excited semiconductor. Palladium is therefore an efficient modifier to be decorated on the semiconductor for the enhancement of photocatalytic activity in photocatalytic reactions.[27,28] By means of constructing a heterostructure with another semiconductor, photogenerated electrons of TNTs could transfer to the conduction band of the coupled semiconductor, which would promote charge separation.[29,30]

Received: May 25, 2018
Revised: August 26, 2018
Published: September 7, 2018

DOI: 10.1021/acssuschemeng.8b02375
ACS Sustainable Chem. Eng. 2018, 6, 12953−12960

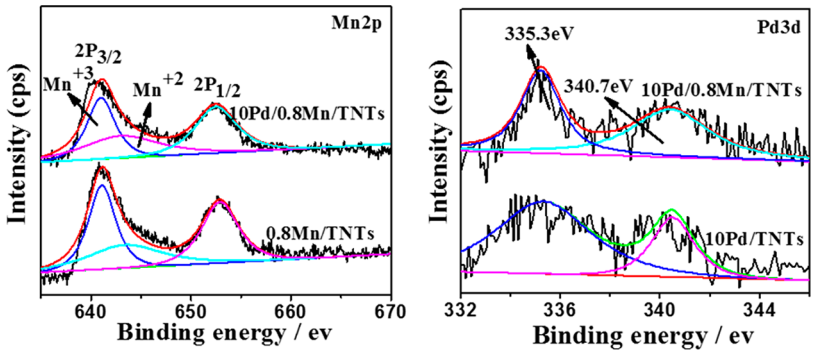

Figure 1. XPS spectra of different photoelectrodes. Mn 2p spectra of 10Pd/0.8Mn/TNTs and 0.8Mn/TNTs photoelectrodes. Pd 3d spectra of 10Pd/0.8Mn/TNTs and 10Pd/TNTs photoelectrodes. The number 0.8 in 10Pd/0.8Mn/TNTs and 0.8Mn/TNTs stands for the used mass of $KMNO_4$. The number 10 in 10Pd/TNTs and 10Pd/0.8Mn/TNTs stands for the electrochemical deposition time of Pd.

Previous studies have looked at elevating the photocatalytic performance of TNTs via one-directional modulation, by improving performance via photogenerated electrons or by holes.[31,32] Unfortunately, only a few studies have shown enhanced photocatalytic properties via bidirectional modulation from both the sides of photogenerated electrons and holes.[33,34] The importance of the oxidation and reduction reactions in the photocatalytic process involved with the photogenerated holes and electrons is still not clear. It is common to modify materials for photocatalysis to improve one-directional transfer by either improving electron transfer or holes. However, the simultaneous control of electrons and holes based on a bidirectional mechanism is more effective. When a modifier to transfer photogenerated electrons is used to decorate a semiconductor, the transport of electrons is facilitated, and more photogenerated electrons can take part in the reduction reaction; thus, performance is enhanced. Apart from promoting the effective charge separation from the photogenerated electron direction, using a modifier to trap the photogenerated holes of a semiconductor could further promote the activity. Since the •OH produced by the reaction of holes with H_2O is an important intermediate in the process of CO_2 reduction, the enhanced concentration of photogenerated holes is needed for efficient production of •OH and effective CO_2 conversion. Therefore, it can be deduced that a bidirectional modulation would have advantages over a one-directional modulation.

To improve photocatalytic activity through bidirectional modulation, we previously fabricated chloride and phosphate codecorated rutile TiO_2 nanorods, and then coupled them with carbon nanotubes.[34] We showed the photocatalytic performance of the modified rutile TiO_2 was elevated because the holes captured by the surface negative field formed with the modified chloride and phosphate groups, and the electron transfer accelerated by the carbon nanotubes, thus improving charge separation. This demonstrated that it was important to elevate charge separation for modulation of the photogenerated electrons and holes via a bidirectional modulation mechanism during the photocatalytic process. Hence, it is a viable and valid approach for elevating photocatalytic activity of the TNTs photoelectrode by codecoration with MnO_x and palladium to simultaneously control the photogenerated holes and electrons on the TNTs photoelectrode.

TNTs photoelectrodes were codecorated here with MnO_x and Pd via a straightforward impregnation approach and electrochemical deposition method. The effects of codecoration with MnO_x and Pd were examined on the photoelectrochemical properties and photocatalytic activities of TNTs, and compared to controls lacking these additional materials. It was demonstrated that the photocatalytic performance for CO_2 conversion was vastly elevated based on the bidirectional control mechanism from both sides of photogenerated electrons and holes. This work affords us a valid means to elevate the charge separation of TNTs-based photocatalysts via bidirectional control of the photogenerated holes and electrons for the application of energy production.

RESULTS AND DISCUSSION

The surface compositions and structures of the synthetic photoelectrodes with and without modification were analyzed using XRD (Figure S1). Three phases of titanium were observed including anatase phase labeled with A, rutile phase labeled with R, and metal phase labeled with T.[27,35] The crystal phase of TNTs photoelectrodes did not change after further codecoration with MnO_x and Pd. The optical absorption of the photoelectrodes with and without modification was also examined (Figure S2). For the bare TNTs photoelectrode, evidence of the absorption of UV and visible light could be seen based on the wide band gap energy of TiO_2 and the nanotubular structure.[27,36] With the modification of MnO_x and Pd, the light absorption ability of TNTs was elevated, and the 10Pd/0.8Mn/TNTs photoelectrode showed a higher UV and visible light absorption intensity than bare TNTs, Pd decorated TNTs, and MnO_x decorated TNTs. For calculation of the band gap energy of the synthetic photoelectrodes and investigation of the change of the optical absorption abilities in detail, the relationship between $[F(R)h\nu]^{1/2}$ and $h\nu$ was explored (Figure S2B), in which $F(R) = (1 - R)^2/(2R)$, and R stands for the percentage of light reflected by the material.[37] By making the tangent lines of the curves extend to the X-axis, the E_g values of bare TNTs, 0.8Mn/TNTs, 10Pd/TNTs, and 10Pd/0.8Mn/TNTs photoelectrodes were obtained to be 3.01, 2.72, 2.67, and 2.62 eV, respectively. The evident band gap change of the 10Pd/0.8Mn/TNTs photoelectrode was on account of the decorated brown MnO_x and Pd benefiting from light absorption in the visible region.[38] The significantly enhanced visible light absorption made the 10Pd/0.8Mn/TNTs photoelectrode a potential solar-light driven photocatalyst.

According to the XPS measurements (Figure 1 and Figure S3), Ti and O elements existed on all photoelectrodes. There were two peaks resulted from Ti^{4+} in the Ti 2p spectra, including the Ti $2p_{1/2}$ peak with a binding energy of 464.1 eV, and the Ti $2p_{3/2}$ peak with a binding energy of 458.3 eV. In the spectra of O

DOI: 10.1021/acssuschemeng.8b02375
ACS Sustainable Chem. Eng. 2018, 6, 12953−12960

1s XPS, the broad peak could be divided into a strong peak with a binding energy of 529.5 eV and a shoulder peak with a binding energy of 531.8 eV. The peak at the location of 529.5 eV was on account of the Ti−O−Ti lattice oxygen, and the peak at 531.8 eV was attributed to the surface hydroxyl oxygen.[39,40] The content of the surface hydroxyl oxygen increased after decoration with MnO_x and Pd. The MnO_x and Pd codecorated TNTs photoelectrode exhibited the highest content of hydroxyl groups, indicating that the oxygen vacancies which could play a part of elevating the visible light absorption and enhance the charge separation were generated during the processing of decorated TNTs.[41] Elemental Mn was also detected in the 0.8Mn/TNTs and 10Pd/0.8Mn/TNTs photoelectrodes. From the Mn 2p spectra, it can be deduced that elemental Mn presented with the oxidation states of Mn^{2+} and Mn^{3+} which was consistent with a previous study.[42] Elemental Pd was also measured in the 10Pd/TNTs and 10Pd/0.8Mn/TNTs photoelectrodes. The peaks with the binding energies of approximately 335.3 and 340.7 eV were derived from Pd $3d_{3/2}$ and Pd $3d_{5/2}$, respectively, confirming that Pd^0 was the major form of Pd.[27,43]

Based on analysis using SEM, TEM, and high-resolution TEM (HRTEM) images, the TNTs synthesized with electrochemical anodization of Ti foils produced a highly ordered tubular structure. The inner diameter of the tubular structure was approximately 120 nm, and the wall thickness was 20 nm (Figure 2A). Cross-sectional images (Figure 2B) showed the tube length was about 1 μm. After decorating the TNTs with MnO_x and Pd, the tubular structure was not affected, and the surfaces of the TNTs were covered by flowerlike MnO_x structures and numerous Pd nanoparticles (Figure 2C). From the cross-sectional view of 10Pd/0.8Mn/TNTs (Figure 2D), it can be seen that there were no MnO_x and Pd nanoparticles on the walls of TNTs. Elemental mapping (Figure 2E−H) and energy-dispersive X-ray (EDX) spectroscopy (Figure S4) showed that Ti, O, Mn, and Pd elements were uniformly distributed on the surfaces of the 10Pd/0.8Mn/TNTs photoelectrodes. From examination of the HRTEM image, the crystallized TNTs walls had a lattice spacing of approximately 0.35 nm based on the (101) plane of anatase TiO_2 (Figure S5). These analyses showed that MnO_x and Pd were successfully decorated onto the TNTs photoelectrodes.

A series of photoelectrochemical measurements of TNTs were conducted to examine photogenerated charge separation of the semiconductors. Adding MnO_x enhanced photocurrent intensities (Figure 3A), and the photocurrent intensity of TNTs was enhanced after decorating with Pd. The introduction of Pd in 0.8Mn/TNTs further increased the photocurrent intensity while the corresponding dark currents were essentially unchanged, indicating that the photogenerated charge separation of 10Pd/0.8Mn/TNTs was accordingly high. After codecoration, the photogenerated holes could be effectively trapped by MnO_x, and the photogenerated electron transport could be efficiently enhanced by Pd, leading to elevated photogenerated charge carriers and photocurrent intensity.

The transient photocurrent response was also examined, and the results supported an increase in photocurrent intensity (Figure 3B). All of the photoelectrodes showed a stable and reproducible photocurrent response with on and off cycles using a xenon lamp. When the xenon lamp was turned off, the photocurrent rapidly declined to zero, and it quickly resumed when the light was turned on. The transient photocurrent response of 10Pd/0.8Mn/TNTs (1.15 mA cm^{-2}) was about 2.2

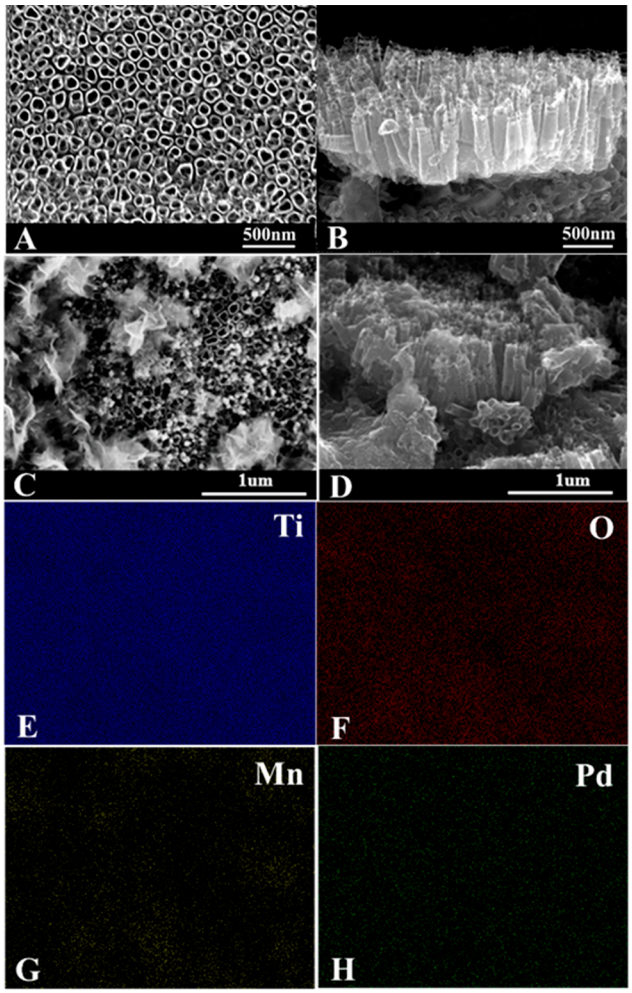

Figure 2. (A) Top and (B) cross-sectional SEM images of the TNTs photoelectrode without modification. (C) Top and (D) cross-sectional SEM images of the MnO_x and Pd codecorated TNTs photoelectrode (10Pd/0.8Mn/TNTs). (E−H) Element mapping of the 10Pd/0.8Mn/TNTs photoelectrode.

times that of the bare TNTs (0.53 mA cm^{-2}), and was higher than the best performing TNTs decorated with MnO_x (0.8Mn/TNTs, 0.66 mA cm^{-2}) or Pd (10Pd/TNTs, 0.91 mA cm^{-2}), showing codecoration with MnO_x and Pd further elevated photogenerated charge separation.

Electrochemical impedance spectroscopy (EIS) measurements of bare and decorated TNTs photoelectrodes were obtained with and without light irradiation (Figure 3C,D). The equivalent circuit based on $R_s(C_{dl}(R_{ct}W))$ was used to fit the impedance spectra (Table S1), where R_s is the solution resistance of the electrolyte between the two electrodes and the double layer capacitance (C_{dl}), R_{ct} is the charge transfer resistance, and W is the Warburg impedance (Figure S6). The interface charge transfer resistance (R_{ct}) values of TNTs, 0.8Mn/TNTs, 10Pd/TNTs, and 10Pd/0.8Mn/TNTs photoelectrodes were observed to be 1.174×10^5, 8.518×10^4, 7.742×10^4, and 6.594×10^4 Ω, respectively, in the dark. However, under light irradiation, the charge transfer resistance (R_{ct}) of TNTs greatly decreased with codecoration of MnO_x and Pd. The interface charge transfer resistance (R_{ct}) values of TNTs, 0.8Mn/TNTs, 10Pd/TNTs, and 10Pd/0.8Mn/TNTs photoelectrodes were 4.124×10^4, 117.1, 30.47, and 1.803 Ω, respectively, indicating that the 10Pd/0.8Mn/TNTs photo-

DOI: 10.1021/acssuschemeng.8b02375
ACS Sustainable Chem. Eng. 2018, 6, 12953−12960

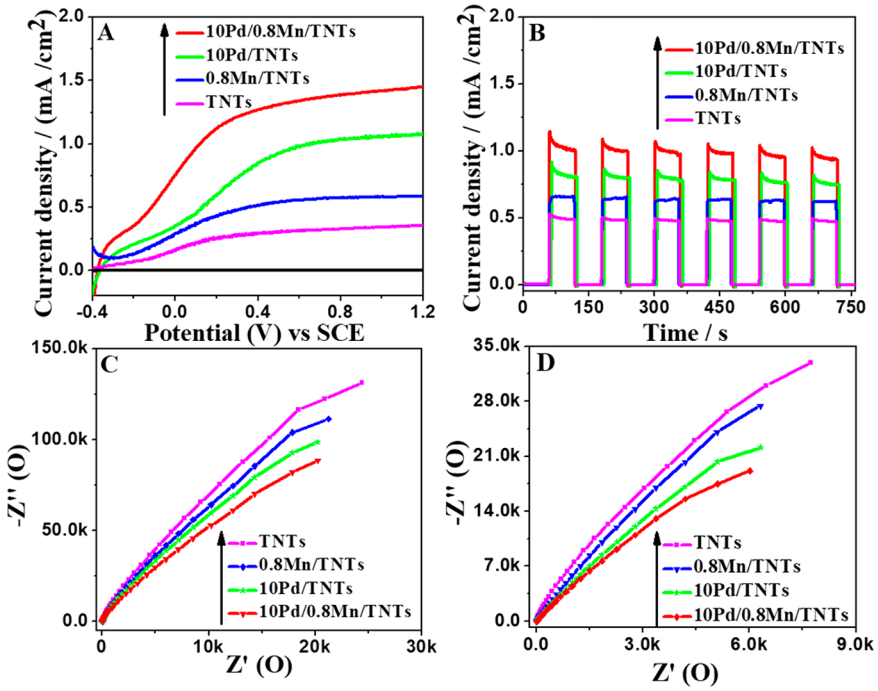

Figure 3. (A) Photocurrent response of different photoelectrodes, in which the black lines were tested without light irradiation, and the colorful lines were tested with light irradiation. (B) Transient photocurrent response of bare and decorated TNTs photoelectrodes. Electrochemical impedance spectra tested (C) without and (D) with light irradiation.

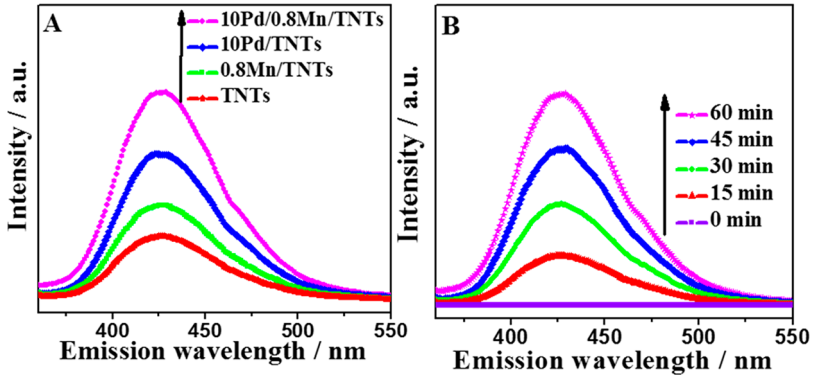

Figure 4. (A) Comparative fluorescence spectra of bare and decorated TNTs photoelectrodes. (B) Fluorescence spectra of the 10Pd/0.8Mn/TNTs photoelectrode with different light irradiation times.

electrode had a much better electron transfer capacity compared with the bare TNTs photoelectrode, thereby resulting in a good photocatalytic performance for CO_2 reduction.

During the photocatalytic process, the produced •OH is an important component of the reactions. The concentration of •OH can reflect the photogenerated separation of electrons and holes. Thus, the produced •OH was monitored for evaluating charge separation. The fluorescence intensities of 2-hydroxyterephthalic acid (TAOH) at a fixed exposure of 1 h on the bare TNTs were compared to the decorated TNTs under xenon lamp irradiation (Figure 4A and Figure S7). The MnO_x decoration enhanced the fluorescence intensity of the TNTs. The fluorescence intensity of TNTs was also enhanced by decorating with a suitable amount of Pd. The introduction of Pd in 0.8Mn/TNTs was favorable for the enhanced fluorescence intensity, demonstrating that the produced •OH on 10Pd/0.8Mn/TNTs photoelectrode should be the largest among the four different photoelectrodes, corresponding to the highest charge separation. The elevated •OH concentration was due to the elevated charge separation and light absorption ability. The data on the produced concentrations of hydroxyl •OH radicals were consistent with the improved photocurrent density above, confirming that the photogenerated charge separation of TNTs was elevated via codecorating with a proper amount of MnO_x and Pd. For a study of the change of the produced •OH radicals with extending the irradiation, the fluorescence intensity under xenon lamp irradiation for 1 h on 10Pd/0.8Mn/TNTs was also investigated (Figure 4B). The fluorescence intensity was elevated at an emission wavelength of 425 nm when the irradiation time was prolonged to 1 h.

Based on the above series of tests which demonstrated that codecoration with MnO_x and Pd improved charge separation of TNTs, it was expected that this would increase photocatalytic CO_2 conversion (Figure 5). For the bare TNTs photoelectrode, acetic acid, methanol, and formic acid were the major products. For decorated TNTs photoelectrodes, methanol disappeared, and acetic acid and formic acid were the major products. After MnO_x decoration, the photocatalytic CO_2 conversion of TNTs

DOI: 10.1021/acssuschemeng.8b02375
ACS Sustainable Chem. Eng. 2018, 6, 12953−12960

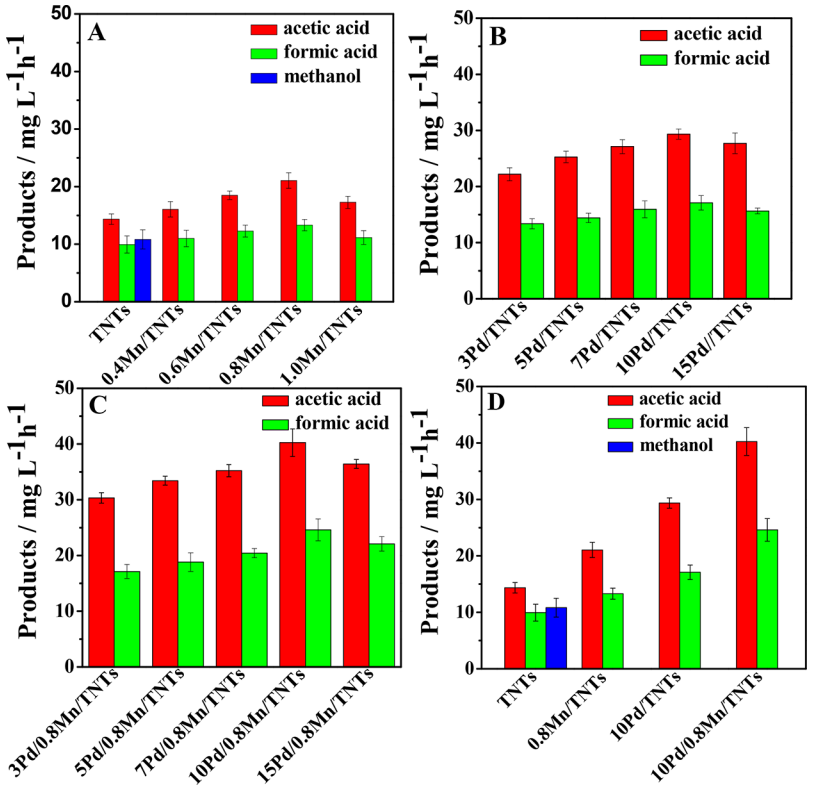

Figure 5. Photocatalytic activities for CO_2 conversion in $KHCO_3$ aqueous solution with a concentration of 0.1 M on different photoelectrodes, under xenon lamp irradiation for 1 h. (A) Bare TNTs and MnO_x decorated TNTs. The numbers 0.4, 0.6, 0.8, and 1.0 indicate the used mass of $KMnO_4$. (B) Pd decorated TNTs. The numbers 3, 5, 7, 10, and 15 indicate the electrochemical deposition time of Pd. (C) MnO_x and Pd codecorated TNTs. The numbers 3, 5, 7, 10, and 15 indicate the electrochemical deposition time of Pd. (D) Comparison of four different photoelectrodes, bare TNTs, MnO_x decorated TNTs, Pd decorated TNTs, and MnO_x and Pd codecorated TNTs.

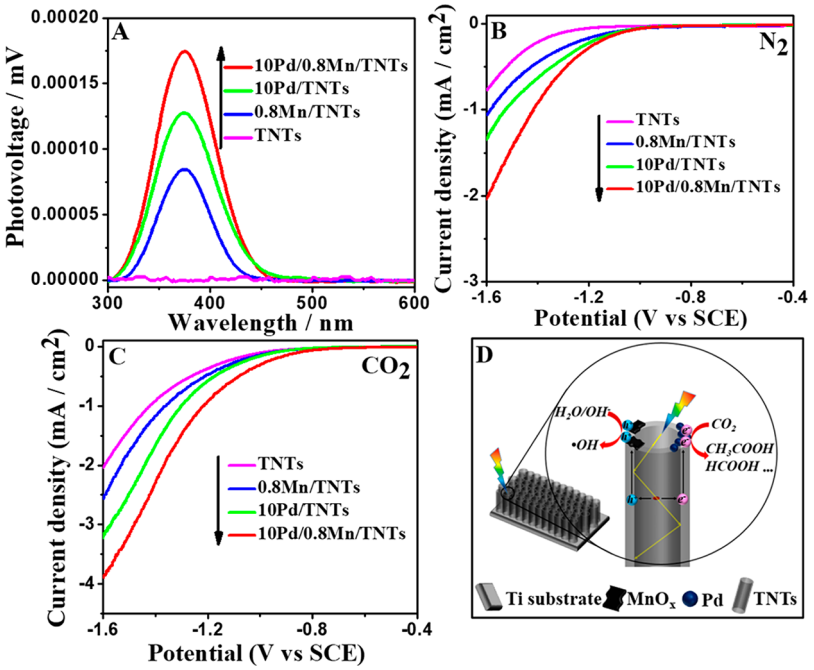

Figure 6. (A) SPS responses of bare and decorated TNTs photoelectrodes in N_2. Electrochemical reduction curves of bare and decorated TNTs photoelectrodes (B) in a nitrogen-bubbled system and (C) in a carbon-dioxide-bubbled system. (D) Charge transfer and separation scheme on the MnO_x and Pd codecorated TNTs photoelectrode involved in the CO_2 reduction reaction.

photoelectrodes was enhanced. As the amount of $KMnO_4$ used increased, the concentrations of acetic acid and formic acid increased and then declined. The optimal performance was obtained with 0.8 g of $KMnO_4$ (0.8Mn/TNTs), with 21.1 ± 1.3 mg L^{-1} acetic acid and 13.3 ± 0.9 mg L^{-1} formic acid. Similarly, the photocatalytic activity of TNTs was also elevated after

DOI: 10.1021/acssuschemeng.8b02375
ACS Sustainable Chem. Eng. 2018, 6, 12953−12960

decorating with Pd, with an increase and then a decrease in yields of acetic and formic acids for electrodeposition times of 3−15 min. The best results were obtained when the electrodeposition time was 10 min (10Pd/TNTs), based on the production of acetic acid with a concentration of 29.4 ± 0.9 mg L^{-1} and formic acid with a concentration of 17.1 ± 1.3 mg L^{-1}. The introduction of Pd onto the 0.8Mn/TNTs photoelectrode further enhanced photocatalytic activity. When the electrodeposition time was 10 min (10Pd/0.8Mn/TNTs), the photoelectrode exhibited the highest activity for the production of acetic (40.3 ± 2.5 mg L^{-1}) and formic (24.6 ± 1.9 mg L^{-1}) acids, which were ∼2.8 times and ∼2.5 times enhanced compared to bare TNTs. The evaluated photocatalytic activities were consistent with the corresponding photocurrent density and •OH radical production results shown above.

For confirmation that the carbon atoms in the produced acetic acid and formic acid were indeed derived from CO_2, N_2 was used to replace CO_2 for the photocatalytic activity tests in a $KHCO_3$ solution (0.1 M) with the 10Pd/0.8Mn/TNTs photoelectrode. When N_2 was sparged into the solution, no product was detected. However, when CO_2 was sparged into the solution, both acetic acid (41.2 mg L^{-1} h^{-1}) and formic acid (25.4 mg L^{-1} h^{-1}) were detected after xenon lamp irradiation for 1 h (Figure S8). Thus, it can be deduced that the carbon atoms in acetic acid and formic acid were indeed derived from CO_2. The proposed mechanism for the number of electrons involved during the formation of formic acid and acetic[44] is

$$CO_2 + 2H^+ + 2e^- \rightarrow HCOOH\ (-0.58\ V\ vs\ NHE) \quad (1)$$

$$2CO_2 + 8H^+ + 8e^- \rightarrow CH_3COOH + 2H_2O\ (-0.31\ V\ vs\ NHE) \quad (2)$$

The stability test of the 10Pd/0.8Mn/TNTs photoelectrode was also investigated (Figure S9). The production for CO_2 conversion with the 10Pd/0.8Mn/TNTs photoelectrode was nearly kept unchanged after 7 cycles of experiments, demonstrating good stability of the resulting modified TNTs photoelectrode.

To further investigate the charge separation mechanism, surface photovoltage spectroscopy (SPS) analysis was conducted (Figure 6A and Figure S10). The SPS response of TNTs was enhanced by increasing the amount of MnO_x, which was attributed to the function of trapping holes by the decorated MnO_x. The 0.8Mn/TNTs showed the highest SPS response among all MnO_x samples. The SPS response of TNTs was also enhanced after decorating with Pd, with the best result obtained using 10Pd/TNTs due to the function of an improved transfer of electrons. The SPS response of TNTs was further enhanced by codecorating them with MnO_x and Pd, with the best response obtained with 10Pd/0.8Mn/TNTs. The enhanced SPS response was therefore due to the Pd improving electron transfer and the decorated MnO_x trapping holes, leading to greatly enhanced photogenerated charge separation.

The electrochemical reduction experiments on TNTs, 0.8Mn/TNTs, 10Pd/TNTs, and 10Pd/0.8Mn/TNTs photoelectrodes were also tested in CO_2 and N_2 environments, respectively (Figure 6B,C). In the N_2-bubbled system, electrochemical H_2 evolution on 0.8Mn/TNTs and 10Pd/TNTs was improved compared to plain TNTs, and was further improved by codecoration with MnO_x and Pd. The onset potentials of the different photoelectrodes for CO_2 reduction shifted positively, compared to those for H_2 evolution, showing the more favorable reaction for CO_2 reduction compared to H_2 evolution. The addition of MnO_x and Pd therefore played catalytic roles in the redox reactions involved with the photogenerated charge carriers as well as improving charge separation.

Based on the above results, an overall scheme was summarized (Figure 6D). When the TNTs photoelectrode was illuminated with the xenon lamp, the light was reflected several times inside the tubular structure of TNTs, and the photogenerated electrons and holes were formed. The produced photogenerated holes and electrons could diffuse along the pipe wall of TNTs to the surface, where they were captured by MnO_x and Pd. The photogenerated holes with strong oxidation properties could react with OH^- or H_2O, resulting in •OH radicals formed. The photogenerated electrons then reacted with CO_2 to produce chemical compounds. The enhanced photocatalytic performance was a result of the improved bidirectional control of photogenerated charges. The decoration of MnO_x could more effectively trap photogenerated holes, and decoration with Pd facilitated photogenerated electron transfer and promoted visible light absorption. The catalytic roles introduced in the redox reactions involved with the photogenerated charge carriers by MnO_x and Pd also resulted in improved photocatalytic activities for CO_2 conversion.

CONCLUSION

TNTs codecorated with MnO_x and Pd effectively trapped photogenerated holes, facilitated photogenerated electron transfer, and promoted visible light absorption. The photogenerated charge separation was greatly elevated by this bidirectional modulation. The codecoration of MnO_x and Pd also played catalytic roles in the redox reactions involved with the photogenerated charge carriers as well as improving charge separation, leading to greatly improved photocatalytic CO_2 conversion. This strategy of modulating photogenerated electrons and holes based on bidirectional modulation was shown to be highly feasible and effective for photocatalysis of CO_2 to chemical products, and thus it could be a viable method for other TNTs photocatalysts applied to energy production.

ASSOCIATED CONTENT

Supporting Information

The Supporting Information is available free of charge on the ACS Publications website at DOI: 10.1021/acssuschemeng.8b02375.

Additional details and figures including XRD patterns, UV−vis absorption reflectance spectra, Tauc plots, EDX results, TEM image, HRTEM image, Nyquist plots, fluorescence spectra, and SPS responses (PDF)

AUTHOR INFORMATION

Corresponding Authors

*E-mail: jia14921@163.com.

*E-mail: yujief@hit.edu.cn. Phone: (+86) 451-86287017. Fax: (+86) 451-86287017.

ORCID

Yujie Feng: 0000-0001-8342-5482

Notes

The authors declare no competing financial interest.

ACKNOWLEDGMENTS

This work was supported by the National Key R&D Program of China (Grant 2016YFE0106500), National Natural Science

Fund of China (Grant 21673061 and 51408156). The authors also acknowledge the International Cooperating Project between China and European Union (Grant 2014DFE90110).

REFERENCES

(1) Xu, Y.; Jia, Y.; Zhang, Y.; Nie, R.; Zhu, Z.; Wang, J.; Jing, H. Photoelectrocatalytic reduction of CO_2 to methanol over the multi-functionalized TiO_2 photocathodes. *Appl. Catal., B* **2017**, *205*, 254−261.

(2) Jiang, Z.; Liang, X.; Zheng, H.; Liu, Y.; Wang, Z.; Wang, P.; Zhang, X.; Qin, X.; Dai, Y.; Whangbo, M. H.; Huang, B. Photocatalytic reduction of CO_2 to methanol by three-dimensional hollow structures of Bi_2WO_6 quantum dots. *Appl. Catal., B* **2017**, *219*, 209−215.

(3) Pan, Y.-X.; You, Y.; Xin, S.; Li, Y.; Fu, G.; Cui, Z.; Men, Y.-L.; Cao, F.-F.; Yu, S.-H.; Goodenough, J.-B. Photocatalytic CO_2 Reduction by Carbon-Coated Indium-Oxide Nanobelts. *J. Am. Chem. Soc.* **2017**, *139*, 4123−4129.

(4) Li, K.; Peng, B.; Peng, T. Recent Advances in Heterogeneous Photocatalytic CO_2 Conversion to Solar Fuels. *ACS Catal.* **2016**, *6*, 7485−7527.

(5) Bai, S.; Jiang, J.; Zhang, Q.; Xiong, Y. Steering charge kinetics in photocatalysis: intersection of materials syntheses, characterization techniques and theoretical simulations. *Chem. Soc. Rev.* **2015**, *44*, 2893−2939.

(6) Zhang, G.; Liu, G.; Wang, L.; Irvine, J. T. S. Inorganic perovskite photocatalysts for solar energy utilization. *Chem. Soc. Rev.* **2016**, *45*, 5951−5984.

(7) Sheng, X.; Liu, Z.; Zeng, R.; Chen, L.; Feng, X.; Jiang, L. Enhanced Photocatalytic Reaction at Air-Liquid-Solid Joint Interfaces. *J. Am. Chem. Soc.* **2017**, *139*, 12402−12405.

(8) Kumar, R.; Govindarajan, S.; Siri Kiran Janardhana, R. K.; Rao, T. N.; Joshi, S. V.; Anandan, S. Facile One-Step Route for the Development of in Situ Cocatalyst-Modified Ti^{3+} Self-Doped TiO_2 for Improved Visible-Light Photocatalytic Activity. *ACS Appl. Mater. Interfaces* **2016**, *8*, 27642−27653.

(9) Xiang, Q.; Yu, J.; Jaroniec, M. Synergetic effect of MoS_2 and graphene as cocatalysts for enhanced photocatalytic H_2 production activity of TiO_2 nanoparticles. *J. Am. Chem. Soc.* **2012**, *134*, 6575−6578.

(10) Zeng, M.; Li, Y.; Mao, M.; Bai, J.; Ren, L.; Zhao, X. Synergetic Effect between Photocatalysis on TiO_2 and Thermocatalysis on CeO_2 for Gas-Phase Oxidation of Benzene on TiO_2/CeO_2 Nanocomposites. *ACS Catal.* **2015**, *5*, 3278−3286.

(11) Zhou, X.; Liu, N.; Schmuki, P. Photocatalysis with TiO_2 Nanotubes: "Colorful" Reactivity and Designing Site-Specific Photocatalytic Centers into TiO_2 Nanotubes. *ACS Catal.* **2017**, *7*, 3210−3235.

(12) Chang, X.; Thind, S. S.; Chen, A. Electrocatalytic Enhancement of Salicylic Acid Oxidation at Electrochemically Reduced TiO_2 Nanotubes. *ACS Catal.* **2014**, *4*, 2616−2622.

(13) Hesabi, Z. R.; Allam, N. K.; Dahmen, K.; Garmestani, H. Self-standing crystalline TiO_2 nanotubes/CNTs heterojunction membrane: synthesis and characterization. *ACS Appl. Mater. Interfaces* **2011**, *3*, 952−955.

(14) Moniz, S. J. A.; Shevlin, S. A.; Martin, D. J.; Guo, Z. X.; Tang, J. Visible-light driven heterojunction photocatalysts for water splitting-a critical review. *Energy Environ. Sci.* **2015**, *8*, 731−759.

(15) Wu, L.; Li, F.; Xu, Y.; Zhang, J. W.; Zhang, D.; Li, G.; Li, H. Plasmon-induced photoelectrocatalytic activity of Au nanoparticles enhanced TiO_2 nanotube arrays electrodes for environmental remediation. *Appl. Catal., B* **2015**, *164*, 217−224.

(16) Li, H.; Xia, Z.; Chen, J.; Lei, L.; Xing, J. Constructing ternary CdS/reduced graphene oxide/TiO_2 nanotube arrays hybrids for enhanced visible-light-driven photoelectrochemical and photocatalytic activity. *Appl. Catal., B* **2015**, *168−169*, 105−113.

(17) Luna, A. L.; Novoseltceva, E.; Louarn, E.; Beaunier, P.; Kowalska, E.; Ohtani, B.; Valenzuela, M. A.; Remita, H.; Colbeau-Justin, C. Synergetic effect of Ni and Au nanoparticles synthesized on titania particles for efficient photocatalytic hydrogen production. *Appl. Catal., B* **2016**, *191*, 18−28.

(18) Huang, S.-Z.; Jin, J.; Cai, Y.; Li, Y.; Tan, H.-Y.; Wang, H.-E.; Van Tendeloo, G.; Su, B.-L. Engineering single crystalline Mn_3O_4 nano-octahedra with exposed highly active {011} facets for high performance lithium ion batteries. *Nanoscale* **2014**, *6*, 6819−6827.

(19) Iwase, A.; Yoshino, S.; Takayama, T.; Ng, Y. H.; Amal, R.; Kudo, A. Water Splitting and CO_2 Reduction under Visible Light Irradiation Using Z-Scheme Systems Consisting of Metal Sulfides, CoO_x-Loaded $BiVO_4$, and a Reduced Graphene Oxide Electron Mediator. *J. Am. Chem. Soc.* **2016**, *138*, 10260−10264.

(20) Deng, S.; Meng, T.; Xu, B.; Gao, F.; Ding, Y.; Yu, L.; Fan, Y. Advanced MnO_x/TiO_2 Catalyst with Preferentially Exposed Anatase {001} Facet for LowTemperature SCR of NO. *ACS Catal.* **2016**, *6*, 5807−5815.

(21) Dong, R.; Ye, Q.; Kuang, L.; Lu, X.; Zhang, Y.; Zhang, X.; Tan, G.; Wen, Y.; Wang, F. Enhanced supercapacitor performance of Mn_3O_4 nanocrystals by doping transition metal ions. *ACS Appl. Mater. Interfaces* **2013**, *5*, 9508−9516.

(22) Wang, Y.; Zhu, L.; Yang, X.; Shao, E.; Deng, X.; Liu, N.; Wu, M. Facile synthesis of three-dimensional Mn_3O_4 hierarchical microstructures and their application in the degradation of methylene blue. *J. Mater. Chem. A* **2015**, *3*, 2934−2941.

(23) Liu, Y.; Guo, Y.; Schelhas, L. T.; Li, M.; Ager, J. W. Undoped and Ni-Doped CoO_x Surface Modification of Porous $BiVO_4$ Photoelectrodes for Water Oxidation. *J. Phys. Chem. C* **2016**, *120*, 23449−23457.

(24) Kirner, J. T.; Stracke, J. J.; Gregg, B. A.; Finke, R. G. Visible-light-assisted photoelectrochemical water oxidation by thin films of a phosphonate functionalized perylene diimide plus CoO_x cocatalyst. *ACS Appl. Mater. Interfaces* **2014**, *6*, 13367−13377.

(25) Raziq, F.; Sun, L.; Wang, Y.; Zhang, X.; Humayun, M.; Ali, S.; Bai, L.; Qu, Y.; Yu, H.; Jing, L. Synthesis of Large-Surface-Area g-C_3N_4 Co-modified with MnO_x and Au-TiO_2 as Efficient Visible-Light Photocatalysts for Fuel Production. *Adv. Energy. Mater.* **2018**, *8*, 1701580.

(26) Vaiano, V.; Iervolino, G.; Sannino, D.; Murcia, J. J.; Hidalgo, M. C.; Ciambelli, P.; Navío, J. A. Photocatalytic removal of patent blue V dye on Au-TiO_2 and Pt-TiO_2 catalysts. *Appl. Catal., B* **2016**, *188*, 134−146.

(27) Cheng, X.; Liu, H.; Chen, Q.; Li, J.; Wang, P. Preparation and characterization of palladium nano-crystallite decorated $TiO_{(2)}$ nanotubes photoelectrode and its enhanced photocatalytic efficiency for degradation of diclofenac. *J. Hazard. Mater.* **2013**, *254−255*, 141−148.

(28) Li, J.; Liu, H.; Cheng, X.; Xin, Y.; Xu, W.; Ma, Z.; Ma, J.; Ren, N.; Li, Q. Stability of Palladium-Polypyrrole-Foam Nickel Electrode and Its Electrocatalytic Hydrodechlorination for Dichlorophenol Isomers. *Ind. Eng. Chem. Res.* **2012**, *51*, 15557−15563.

(29) Wang, X.-j.; Yang, W.-y.; Li, F.-t.; Zhao, J.; Liu, R.-h.; Liu, S. J.; Li, B. Construction of amorphous $TiO_{(2)}$/BiOBr heterojunctions via facets coupling for enhanced photocatalytic activity. *J. Hazard. Mater.* **2015**, *292*, 126−136.

(30) Su, J.; Zhu, L.; Geng, P.; Chen, G. Self-assembly graphitic carbon nitride quantum dots anchored on TiO_2 nanotube arrays: An efficient heterojunction for pollutants degradation under solar light. *J. Hazard. Mater.* **2016**, *316*, 159−168.

(31) Wang, J.; Qin, C.; Wang, H.; Chu, M.; Zada, A.; Zhang, X.; Li, J.; Raziq, F.; Qu, Y.; Jing, L. Exceptional photocatalytic activities for CO_2 conversion on Al-O bridged g-C_3N_4/α-Fe_2O_3 z-scheme nanocomposites and mechanism insight with isotopesZ. *Appl. Catal., B* **2018**, *221*, 459−466.

(32) Li, J.; Zhang, X.; Raziq, F.; Wang, J.; Liu, C.; Liu; Sun, Y. J.; Yan, R.; Qu, B.; Qin, C.; Jing, L. Improved photocatalytic activities of g-C_3N_4 nanosheets by effectively trapping holes with halogen-induced surface polarization and 2,4-dichlorophenol decomposition mechanism. *Appl. Catal., B* **2017**, *218*, 60−67.

(33) Liu, Y.; Wu, J.; Lu, H.; Wang, J.; Qu, Y.; Jing, L. Enhanced photocatalytic activities of commercial P25 TiO_2 by trapping holes and transferring electrons for CO_2 conversion and 2,4-dichlorophenol degradation. *Mater. Res. Bull.* **2017**, *92*, 23−28.

DOI: 10.1021/acssuschemeng.8b02375
ACS Sustainable Chem. Eng. 2018, 6, 12953−12960

(34) Wu, J.; Lu, H.; Zhang, X.; Raziq, F.; Qu, Y.; Jing, L. Enhanced charge separation of rutile TiO_2 nanorods by trapping holes and transferring electrons for efficient cocatalyst-free photocatalytic conversion of CO_2 to fuels. *Chem. Commun.* **2016**, *52*, 5027−5029.
(35) Yu, J.; Dai, G.; Cheng, B. Effect of Crystallization Methods on Morphology and Photocatalytic Activity of Anodized TiO_2 Nanotube Array Films. *J. Phys. Chem. C* **2010**, *114*, 19378−19385.
(36) Zhou, X.; Liu, N.; Schmuki, P. Photocatalysis with TiO_2 Nanotubes: Colorful Reactivity and Designing Site-Specific Photocatalytic Centers into TiO_2 Nanotubes. *ACS Catal.* **2017**, *7*, 3210−3235.
(37) Bjelajac, A.; Djokic, V.; Petrovic, R.; Socol, G.; Mihailescu, I. N.; Florea, I.; Ersen, O.; Janackovic, D. Visible light-harvesting of TiO_2 nanotubes array by pulsed laser deposited CdS. *Appl. Surf. Sci.* **2014**, *309*, 225−230.
(38) Ru, Y.; Yang, L.; Li, Y.; Jiang, W.; Li, Y.; Luo, Y.; Yang, L.; Li, T.; Luo, S. Photoelectrocatalytic reduction of CO_2 on titania nanotube arrays modified by Pd and RGO. *J. Mater. Sci.* **2018**, *53*, 10351−10362.
(39) Wu, J.; Cui, H.; Zhang, X.; Luan, Y.; Jing, L. Enhanced photocatalytic activity of Cl-residual rutile TiO_2 nanorods after targeted co-modification with phosphoric and boric acids. *Phys. Chem. Chem. Phys.* **2015**, *17*, 15837−15842.
(40) Pei, Z.; Zhu, M.; Huang, Y.; Xue, Q.; Geng, H.; Zhi, C. Dramatically improved energy conversion and storage efficiencies by simultaneously enhancing charge transfer and creating active sites in MnO_x/TiO_2 nanotube composite electrodes. *Nano Energy* **2016**, *20*, 254−263.
(41) Song, J.; Zheng, M.; Yuan, X.; Li, Q.; Wang, F.; Ma, L.; You, Y.; Liu, S.; Liu, P.; Jiang, D.; Ma, L.; Shen, W. Electrochemically induced Ti^{3+} self-doping of TiO_2 nanotube arrays for improved photoelectrochemical water splitting. *J. Mater. Sci.* **2017**, *52*, 6976−6986.
(42) Wang, F.; Dai, H.; Deng, J.; Bai, G.; Ji, K.; Liu, Y. Manganese Oxides with Rod, Wire, Tube, and Flower-Like Morphologies: Highly Effective Catalysts for the Removal of Toluene. *Environ. Sci. Technol.* **2012**, *46*, 4034−4041.
(43) Kidambi, S.; Bruening, M. L. Multilayered Polyelectrolyte Films Containing Palladium Nanoparticles: Synthesis, Characterization, and Application in Selective Hydrogenation. *Chem. Mater.* **2005**, *17*, 301−307.
(44) Murugesan, P.; Narayanan, S.; Manickam, M.; Murugesan, P. K.; Subbiah, R. A direct Z-scheme plasmonic AgCl@g-C_3N_4 heterojunction photocatalyst with superior visible light CO_2 reduction in aqueous medium. *Appl. Surf. Sci.* **2018**, *450*, 516−526.

DOI: 10.1021/acssuschemeng.8b02375
ACS Sustainable Chem. Eng. 2018, 6, 12953−12960